Icosahedral superstrength at the nanoscale

Cody Kunka, Xiaokun Yang, Qi An, and Ghatu Subhash

Phys. Rev. Materials **2**, 063606 — Published 27 June 2018

DOI: 10.1103/PhysRevMaterials.2.063606

Icosahedral Superstrength at the Nanoscale

[1]Cody Kunka, [2]Xiaokun Yang, [2,3]Qi An, [1]Ghatu Subhash*
[1]Mechanical and Aerospace Engineering, University of Florida, Gainesville, FL 32611 USA
[2]Chemical and Materials Engineering, University of Nevada, Reno, Reno, NV 89557 USA
[3]Nevada Institute for Sustainability, University of Nevada, Reno, Reno, Nevada 89557 USA

Abstract

Materials that exhibit extreme hardness, low mass density, and high thermal/chemical stability can often be modeled as simple modifications to the α-rhombohedral phase of boron. To facilitate the development and discovery of these multipurpose, structural ceramics, the current work reveals fundamental physics on the bonding and deformation of p-block hexaborides, an important and representative subclass of icosahedral solids. Icosahedral separation and localization of equatorial bonding are identified as predictors of both elastic moduli and strength. This work also explores nanotwinning, an advanced nanostructure responsible for dramatic records in mechanical performance of both metals and ceramics. To help develop the first model of nanotwinning in ceramics, this work demonstrates (1) that susceptibility to nanotwinning relies on key bonding traits and (2) that nanotwinning minimally affects elasticity and high-periodicity inelasticity. Overall, this work helps rationalize both the mechanical performance of a major class of materials and the cutting-edge mechanism of nanotwinning through fundamental, physics-based approaches.

Keywords

Icosahedra; Hexaborides; Nanotwinning; Hardness; Density Functional Theory

*Corresponding Author: subhash@ufl.edu

Introduction: Modified α-Boron Structures

Many materials that exhibit extreme hardness, low mass density, and high thermal/chemical stability can be viewed as simple modifications to the α-rhombohedral phase of boron [(B_{12})][1-3]. Hence, this manuscript refers to these boron-rich, icosahedral ceramics as a modified α-boron structures (mαB's). The main structural units of most mαB's are fully boron icosahedra directly bonded at all six polar sites of each icosahedron [i.e., (B_{12})]. Without modification, this (B_{12}) has an experimental Vickers microhardness (HV) of 34 GPa, which is lower than a theoretical prediction of 39 GPa[4]. However, note that this phase of boron has been difficult to produce[3].

While some mαB's have icosahedral substitutions [e.g., $(B_{11}C)CBC$], the main differences among mαB's are interstitial atoms placed around the six equatorial sites of each icosahedron. The most important interstitial sites are the centers of each triplet of icosahedra, so many mαB's have two interstitial atoms per icosahedron [e.g., $(B_{12})OO$[5] and $(B_{12})PP$[6]]. Alternatively, some mαB's have one [e.g., $(B_{12})S$[7]], three [e.g., $(B_{12})CBC$[8] and $(B_{12})NBN$[9]], or four [e.g., $(B_{12})BBBB$[10]] interstitial atom(s) per icosahedron. Especially for binary compounds, the interstitial atoms in the mαB's typically come from Groups IV-A (carbon group), V-A (pnictogen group), and VI-A (chalcogen group) of the p-block of the periodic table[3,11].

Group IV-A provides the most prevalent icosahedral solid: boron carbide (B_4C), which has been researched for over fifty years and is employed in numerous fields[12]. Depending on grain size, Vickers microhardness (HV) has varied between 28 and 36 GPa[13,14]. This range is high but lower than the 45-GPa theoretical prediction[15] likely because of nanoscale complexity from extensive polymorphism, defects, and variable stoichiometry (i.e., 8 – 20 at% C)[12]. Most agree that $(B_{12})CBC$[8] and $(B_{11}C)CBC$[16] are the majority constituents, but minority constituents

are frequently debated[10,17,18]. Additionally, these B-C mαB's also accept metals to form ternary compounds. For example, $Mg_x(B_{12})_4(CBC)_2(C_2)_2$, which had a HV of 32 GPa, is essentially a modification to $(B_{12})CBC$[19]. Likewise, Li has been included to form $LiB_{12}PC$[20] (27-GPa HV), $LiB_{13}C_2$[21], and $Li_2B_{12}C_2$[21].

Amorphization, which is shear-induced, localized loss in crystallinity in nanoscale bands, is the dominant failure mechanism of many icosahedral systems, especially B_4C[12,22-25]. To counter this deleterious phenomenon, recent studies have attempted to dope B_4C with Si (Group IV-A) to increase ductility[26]. The goal is to mitigate bending of the CBC chains by locally introducing structures, such as $(B_{11}C)SiSi$[27] or $(B_{10}Si_2)SiSi$[28]. While these Si-containing mαB's have mainly been the subject of theoretical investigations, $Li_2B_{12}Si_2$[29] and $Mg_2B_{12}Si_2$[30] have been produced experimentally. Note that the incorporation of Mg into mαB's has received particular attention due to the BAM (boron aluminum magnesium) materials (e.g., $MgAlB_{14}$), which have excellent frictional properties[31,32].

When boron subnitride (Group V-A) was first discovered, researchers assumed a structure of $(B_{12})NN$ due to similarity of the experimental x-ray diffraction (XRD) with that of another hexaboride[33]. Later analysis of XRD[9,34,35] and phase stability[36,37] instead suggested $(B_{12})NBN$, which resembles $(B_{12})CBC$. However, quantum-mechanical modeling of Gibbs free energy[38] and enthalpy[39] suggested that stability requires a 2:1 mixture of $(B_{12})NBN$ and $(B_{12})NN$. Neither structure is stable alone. Regardless, experimental samples exhibited a bulk modulus of 200±15 GPa[40,41] and a HV of 41 GPa[42]. This hardness is close to the 40-GPa theoretical prediction, which assumed a structure of $(B_{12})NBN$ alone. Finally, theoretical work on ternary, N-containing mαB's predicted that $B_{12}N_2Zn$, $B_{12}N_2Cd$, and $B_{12}N_2Be$ are stable, superhard, and semiconducting mαB's[4]. The theoretical HV values for these materials were

predicted to be 46, 42, and 49 GPa, respectively. That last value is one of the highest of any icosahedral solid.

Unlike boron subnitride, boron subphosphide (also Group V-A) only has one structure: $(B_{12})PP$[6,43-46]. This lack of a three-atom chain [i.e., no $(B_{12})PBP$] is likely responsible for the theoretical ability to recover from much more shear deformation than boron carbide [e.g., $(B_{12})CBC$][47,48]. Experimentally, $(B_{12})PP$ processed from micropowders and nanopowders exhibited HV of 28[49] and 35 GPa[50], respectively. The latter value is close to the theoretical predictions of 35[4] and 37 GPa[15]. This variability due to processing is likely responsible for different bulk moduli in other studies: 179±1[51] and 192±12 GPa[52].

Like boron subphosphide, boron suboxide (Group VI-A) only has one form $[(B_{12})OO]$[5,53,54] and the ability to recover from significantly more shear deformation than B_4C[47]. Recent experimentation revealed a bulk modulus of 243 GPa[55] and HV between 30 and 38 GPa[5,55,56]. The latter value well matches the theoretical prediction of 38 GPa[15] but is lower than another theoretical prediction of 47 GPa[4]. While these values are already extraordinary, boron suboxide is arguably the most promising icosahedral solid because of its theoretical[57,58] and experimental[55] susceptibility to nanotwinning (i.e., periodic twins separated by a nanoscale spacing). Whereas regular twins concentrate stress and decrease mechanical performance, nanotwins have set impressive records for copper (i.e., 1200% increase in yield strength[59,60] and 85% increase in fatigue strength[61]), cubic boron nitride (i.e., 40% increase in microhardness and 140% increase in fracture toughness[62]), and diamond (i.e., 100% increase in microhardness[63]). Overall, boron suboxide is arguably the most promising mαB.

Other mαB's with p-block interstitial elements have been experimentally observed but not characterized much beyond XRD. Arsenic (Group V-A) can form boron subarsenide

[$(B_{12})AsAs$[64,65]] and a composite with boron subphosphide [$(B_{12})(As_{1-x}P_x)_2$[66]]. The relatively low 33-GPa theoretical hardness of $(B_{12})AsAs$[4] suggests these materials will probably receive little attention. Group VI-A provides $(B_{12})S$[7,67], $B_6S_{0.6}$[68], and $(B_{12})SeB$[7,69]. As indicated by the results of the current investigation, elements larger than As and Se are likely too large to act as interstitials in a network of polar-bonded, boron-rich icosahedra (i.e., mαB's).

Objective: Fundamental Bonding Physics

As indicated by the introduction, mαB's have exhibited high potential for structural applications. Interestingly, because many of these compounds are formed with nearby elements, mαB's often form a "continuous series of closely related crystals" in terms of lattice parameters[11]. By quantum-mechanically modeling the ground states and shear deformations of α-boron [(B_{12})] and binary mαB's with two interstitial atoms (*i*) per icosahedron [$(B_{12})ii$], this investigation shows that these mαB's have fundamental trends in mechanical properties as well. By testing all *i* atoms in the p-block of the periodic table, the simulation space includes some of the salient mαB's [i.e., $(B_{12})OO$ and $(B_{12})PP$] and can well represent some of the chief physics of more complicated systems (e.g., ternary systems and compounds with three-atom chains).

In addition to α-boron and these p-block hexaborides, this work also simulates the corresponding nanotwinned variations with minimum twin spacing [i.e., τ-(B_{12}) and τ-$(B_{12})ii$]. Here, τ indicates that the nanotwins are separated by a single layer of icosahedra. This nanotwin spacing is likely close enough to the critical spacing to capture fundamental physics[57]. Recall from the Introduction that nanotwinning in many ways represents the cutting edge of mechanical performance for structural ceramics. Overall, the goal is to establish physics-based metrics of

nanoscale bonding responsible for the mechanical performance and nanotwinning susceptibility of icosahedral solids.

Computational Procedure: Density Functional Theory

To establish these fundamental trends in mechanical properties, this investigation first employs density functional theory (DFT) to model the ground-states of (B_{12}), (B_{12})*ii*, τ-(B_{12})*ii,* and τ-(B_{12}). Although hexagonal and rhombohedral representations are interchangeable, the latter is used throughout this investigation for computational efficiency, easy association with the nomenclature, and consistency with the "α-rhombohedral" phase of boron. Fig. 1 shows examples of the quantum-mechanical bonding of these structures. The α-boron [i.e., (B_{12}) and τ-(B_{12})], which comprises boron icosahedra connected exclusively by polar bonds (PB's), is simulated to isolate the influence of these icosahedra from that of the *i* atoms in (B_{12})*ii* and τ-(B_{12})*ii*. To examine the influence of the interstitial (*i*) atoms, which connect the icosahedra through equatorial bonds (EB's), the identities of these atoms are systematically varied within the entire p-block of the periodic table.

These ground-state simulations are performed with the ABNIT software[70-74], an open-source solver for DFT. Computational details include plane-wave basis sets, periodic boundaries, Troullier-Martins norm-conserving pseudopotentials, the Teter-Pade local-density approximation (LDA)[75] of the exchange-correlation functional, and a 1900-eV cutoff energy. This scheme already successfully revealed the complex composition[17,76] and amorphization[23] of B_4C and the x-ray diffraction[55] of B_6O. Also, these parameters ensure convergence down to 0.1 GPa in elastic moduli for B_6O in the current work. Visualizations of the ground-state bonding and atomic structure are performed with VESTA 3.2.1 and Crystal Maker 9.0.0, respectively.

After equilibration, density functional perturbation theory (DFPT) is performed under the harmonic approximation to compute the natural frequencies and relaxed-ion elastic tensors. If these frequencies are positive, dynamic stability is assumed, and the elastic tensors (C_{ij}) are computed to check elastic stability according to following four criteria for rhombohedral systems[77-79]:

$$C_{11} - |C_{12}| > 0 \quad (1)$$

$$C_{44} > 0 \quad (2)$$

$$2^{-1}C_{33}(C_{11} + C_{12}) - C_{13}^2 > 0 \quad (3)$$

$$2^{-1}C_{44}(C_{11} - C_{12}) - C_{14}^2 - C_{15}^2 = C_{44}C_{66} - C_{14}^2 - C_{15}^2 > 0 \quad (4)$$

For the stable structures, bulk and shear moduli are computed from Hill's arithmetic average of the Reuss (i.e., minimum value) and Voigt (i.e., maximum) approximations[80]. The Reuss approximation (R) assumes uniform stress and provides the lower bound of the elastic moduli. For a hexaboride, the Reuss approximations of bulk (K_R) and shear (G_R) moduli are:

$$K_R = [(C_{11} + C_{12})C_{33} - 2C_{13}^2][C_{11} + C_{12} + 2C_{33} - 4C_{13}]^{-1} \quad (5)$$

$$G_R = \{15c(C_{11} - C_{12})C_{44}C_{66}\}\{2(C_{11} - C_{12})[2(C_{11} + C_{12}) + 4C_{13} + C_{33}]C_{44}C_{66} + 3c[2C_{44}C_{66} + (C_{11} - C_{12})(C_{44} + 2C_{66})]\}^{-1} \quad (6)$$

where $c = C_{33}(C_{11} + C_{12}) - 2C_{13}^2$

Alternatively, the Voigt approximation (V) assumes uniform strain and provides the upper bound for the elastic moduli. For a hexaboride, the Voigt approximations of the bulk (K_V) and shear (G_V) moduli are:

$$K_V = 9^{-1}(2C_{11} + 2C_{12}C_{33} + 4C_{13}) \quad (7)$$

$$G_V = 15^{-1}(2C_{11} + C_{33} - C_{12} - 2C_{13} + 6C_{44} + 3C_{66}) \quad (8)$$

For a structural ceramic, perhaps the most useful estimate of performance is hardness, which is the resistance to penetration. Unfortunately, hardness is not a material property and can vary with testing method. Hence, comparison of simulation and experiment often requires approximations, such as empirical curve fits. This investigation estimates Vickers microhardness (HV) through a function specifically designed for hard, polycrystalline materials[81]:

$$HV \approx 2(G^3K^{-2})^{0.585} - 3\ GPa \quad (9)$$

Although this hardness estimate approximates inelastic effects, the above simulations have been purely elastic. Hence, this work next simulates pure shear, which is a homogeneous flattening that stretches in one direction and compresses perpendicular to that direction. This deformation can reveal ideal shear strength (τ_{max}) and may facilitate an understanding of amorphization, which is widely attributed to shear deformation[22]. Based on a prior B_6O investigation[57], the slip systems for the pure shear of (B_{12})*ii* and τ-(B_{12})*ii* are chosen to be $(001)\langle 2\bar{1}\bar{1}\rangle$ and $(010)\langle 001\rangle$, respectively [see Fig. 2(a) and Fig. 2(b)]. To break the 3c-2e bonds (i.e., three atoms acting as centers of bonding by one electron pair) instead of the stronger 2c-2e bonds, the slip systems for (B_{12}) and τ-(B_{12}) are chosen to be $(101)\langle\bar{1}20\rangle$ and $(010)\langle 001\rangle$, respectively [see Fig. 2(c) and Fig. 2(d)]. From these simulations, plots of true stress versus true strain are produced. Also, toughness is approximated by the area under the plot of engineering stress versus engineering strain until failure strain. Toughness can viewed as work, which equals force times displacement from the original position, so engineering values are more appropriate. Failure strain is chosen to be the strain after which a significant drop of stress occurs[82].

Because computational efficiency is important for high-strain simulations, these shear deformations are performed with the Vienna Ab initio Simulation Package (VASP)[83-86]. Computational parameters include plane-wave-basis sets, periodic boundaries, the projector-

augmented-wave (PAW) method, the Perdew−Burke−Ernzerhof (PBE) exchange-correlation functional, and a 600-eV cutoff energy. This scheme was used in prior work to successfully model the stability and deformation of B_6O with various nanotwin spacings[57].

Results: Ground-State Bonding and Elasticity

Only the p-block hexaborides with interstitial atoms from groups V-A (i.e., pnictogens) and VI-A (i.e., chalcogens) are stable. The instability of $(B_{12})NN$ is consistent with the experimental and theoretical work mentioned in the introduction. For each stable $(B_{12})ii$, the corresponding nanotwinned structure passes the same stability criteria and has similar static energy (ΔE_τ) and elastic moduli (K and G) [see Table I]. This ΔE_τ, which is reported per icosahedron, is the largest component of formation energy[87] so can help predict likelihood of nanotwinning. See that ΔE_τ decreases as the covalent radius of the interstitial atoms (r_i) increases and even slightly favors the nanotwinned structure for B_6O by 3 meV. This susceptibility to nanotwinning is consistent with prior investigations that underscores the appeal of B_6O[55,57,58]. As compared to the energy differences among B_4C polymorphs[17], the small magnitude of this 3-meV ΔE_τ suggests that experimental B_6O samples may contain both nanotwinned and nontwinned regions. This finding is consistent with the HR-TEM of a prior B_6O investigation[55] and highlights the need for systematic processing.

For the structures with dynamic and elastic stability, Table I also presents the bulk moduli (K), shear moduli (G), and estimated Vickers-microhardness values (HV). For B_6O, the simulation well matches experimental measurements of bulk modulus (i.e., 241 vs. 243 GPa[55]) and hardness (i.e., 37 vs. 38 GPa[56]). Likewise, the simulation well matches recent experimental hardness of B_6P (i.e., 37 vs. 35 GPa[50]). However, recall that reported bulk moduli values varied

(e.g., 179[51] and 192 GPa[52]), so the current value of 211 GPa may reveal the theoretical maximum. Overall, the current simulations seem reasonably consistent with experimental evidence of nanotwinning, moduli, and hardness values.

With consistency between simulation and experiment verified, consider the trends in the simulated elastic moduli and estimated hardness values. See that r_i positively correlates with K, G, and HV. To rationalize this trend, Fig. 3 provides visualizations of the distributions of electronic density for the $(11\bar{1})$ planes of (B_{12}) and all stable (B_{12})*ii*. Electronic density and therefore covalent bonding are strongest at the red regions (≥0.7 electrons/Å^3) and absent at the blue regions. Ball-and-stick models are superimposed upon these distributions for ease of understanding. Essentially, these maps bisect icosahedra and *i* atoms. As described below, strength of the polar bonds (PB's) and strength of the equatorial bonds (EB's) drive the trends in elastic moduli. Recall that PB's connect neighboring icosahedra directly while EB's connect icosahedra through *i* atoms.

Within the hexaborides, PB strength offers the strongest correlation with elastic moduli. As r_i increases, PB's lengthen/weaken, moduli and stiffness decrease. See how the PB's weaken near the icosahedra when moving from (B_{12})OO to (B_{12})SS to (B_{12})PP to (B_{12})AsAs [see "P" regions in Fig. 3]. Although (B_{12})OO and (B_{12})SS have the same number of valence electrons, (B_{12})OO has a 50% higher shear modulus and a 20% higher bulk modulus (see Table I). Note that each of these short and highly directional PB's connects two icosahedra, so PB strength is reflected by the center-to-center icosahedral spacing, which is identical to the lattice parameter (a) [see Table I]. Equilibrium spacing of icosahedra is dictated by (B_{12}) [see Fig. 3(a)]. Adding low-period elements, such as oxygen, minimally affects a [see Fig. 3(b)]. However, increasing r_i eventually pushes PB's too far beyond this highly stable configuration [see Fig. 3(c)]. Hence,

structures with large *i* atoms generally have weaker bonds than structures with small *i* atoms. This trend is consistent with the experimental evidence that mαB's form three-atom chains only with small interstitial atoms [e.g., (B_{12})NBN and (B_{12})CBC] (see Introduction).

Although PB's are arguably more important, EB's also contribute directional, covalent bonding. For example, (B_{12}) and (B_{12})OO have similar PB's, but the latter has stronger EB's and a 7% higher bulk modulus [see Fig. 3 and Table I]. Importantly, EB's connect icosahedra through these *i* atoms so should be localized near the icosahedra and not in the central region. See that (B_{12})OO has higher electronic density near the equatorial regions and less electronic density at the central region as compared to (B_{12}), (B_{12})SS, (B_{12})PP and (B_{12})AsAs (see "E" and "C" regions in Fig. 3). The large sizes of the S, P, and As atoms especially force valence electrons away from the E region and into the C region. In other words, increasing r_i lengthens and therefore weakens the EB's.

These trends in elastic moduli (see Table I) and features in ground-state bonding (see Fig. 3) are identical for (B_{12})*ii* and τ-B($_{12}$)*ii*. Essentially, elastic deformation does not provide enough strain for the twin boundaries to interact, so the local bonding environments in nontwinned and nanotwinned structures are effectively identical. This finding is similar to how nanograining minimally affects elasticity in other ceramics. As expected, if nanotwinning affects the mechanical response of mαB's, the effects of nanotwinning will manifest during inelastic deformation.

Results: Shear Deformations

From Table I, note that the 39-GPa HV of (B_{12}) exceeds the 37-GPa HV of (B_{12})OO despite smaller elastic moduli and weaker EB's (see Fig. 3). Perhaps the PB's are much more

important than the EB's, so the ideal icosahedral spacing in (B_{12}) counters the lack of EB's. However, this notion is inconsistent with prior work. Experimentally, HV has favored B_6O by 4 GPa [i.e., 34 GPa[4] for (B_{12}) vs. 38 GPa[56] for (B_{12})OO]. Theoretically, HV has favored B_6O by 8 GPa [i.e., 39 GPa for (B_{12}) vs. 47 GPa for (B_{12})OO][4]. Further, the current investigation has suggested that both PB's and EB's can positively contribute to mechanical performance of hexaborides. Most likely, the current hardness prediction based solely on elastic moduli fails to compare significantly different structures [i.e., (B_{12}) vs. (B_{12})*ii*]. Hence, this investigation now turns to the results of shear deformations.

Fig. 4 plots true shear stress (τ) versus true shear strain (γ) for the structures with dynamic and elastic stability. In contrast to the hardness comparison, see that the (B_{12}) has significantly lower shear strength than (B_{12})OO. This finding is consistent with the aforementioned experimental evidence and with the current notion that EB's mechanically benefit mαB's when small interstitial atoms are incorporated. Ignoring this (B_{12}) exception, the rankings of the simulated structures by τ_{max} match the rankings by K, G, and HV (see Table I). This similarity of elastic and inelastic responses is consistent with the fact that the covalent bonding in ceramics generally resists both elastic and inelastic deformation[88]. In particular, note the superiority of (B_{12})OO over all other p-block hexaborides in terms of τ_{max}. Interestingly, see that the chalcogen hexaborides, especially (B_{12})OO, have higher toughness than the pnictogen hexaborides, such as (B_{12})PP. Perhaps the extra valance electrons from the chalcogen atoms increase bonding with the boron atoms, which are known to bond in complex ways. Overall, these results are consistent with the elasticity trends within hexaborides and validate the growing focus on B_6O[55].

As with the elasticity simulations, the pure-shear deformations seem minimally affected by nanotwinning. Nanotwinning only slightly increases τ_{max} and decreases U (see Table I and Fig. 4]. If nanotwinning benefits icosahedral solids in similar fashion as diamond and cubic boron nitride (see Introduction), a larger difference in τ_{max} would be reasonable. However, these highly periodic DFT simulations (see simulation cells in Fig. 2) may not be able to capture important, low-periodicity features present in experimental samples. For example, cracking and amorphization would likely occur at relatively isolated regions of the sample. If these extremely expensive computational features could be simulated, the benefits of nanotwinning would likely be reflected in the simulated τ_{max}. Regardless, these high-periodicity results are still useful in the development of the first model for nanotwinning in ceramics. Note that the highly directional, covalent bonding of hard ceramics typically strongly resists the dislocation motion commonly thought to be affected by nanotwinning in metals[60]. Hence, nanotwinning of ceramics may be quite different from that of metals[62,89].

Conclusions: Icosahedral Superstrength

Through quantum-mechanical simulations of both ground states and shear deformations, this work provides a generalized, physics-based understanding of elasticity and strength in icosahedral solids. Analysis of ground-state bonding trends reveals two main predictors of elastic moduli: (1) icosahedral separation (i.e., strength of polar bonds) and (2) localization of equatorial bonding (i.e., strength of equatorial bonds). Consistency of trends in ground-state bonding and shear deformation suggests these metrics may apply to strength as well. As for nanotwinning, this work demonstrates (1) that susceptibility to nanotwinning relies on key bonding traits and (2) that nanotwinning minimally affects elasticity and high-periodicity inelasticity. For ceramics,

these findings aid development of the first model of nanotwinning, a cutting-edge mechanism responsible for dramatic records in experimental properties. Alongside a fundamental understanding of bonding physics and processing kinetics, such a model would likely yield the next generation of structural materials.

Acknowledgements
This work is supported by the Army Research Office [W911NF-18-1-0040], National Science Foundation [DGE-1315138 (GRFP: Graduate Research Fellowship Program), ACI-1053575 TG-MSS15006 (XSEDE: Extreme Science and Engineering Discovery Environment), CMMI−1727428], and the US Nuclear Regulatory Commission [NRC-HQ-84-15-G-0028].

References
[1] Z. Zhao, B. Xu, Y. Tian, *Annu. Rev. Mater. Res.* **2016**, 46, 383.
[2] T. Zhu, J. Li, *Prog. Mater. Sci.* **2010**, 55, 710.
[3] B. Albert, H. Hillebrecht, *Angew. Chem. Int. Ed.* **2009**, 48, 8640.
[4] F. Gao, X. Qin, L. Wang, Y. He, G. Sun, L. Hou, W. Wang, *The Journal of Physical Chemistry B.* **2005**, 109, 14892.
[5] M. Herrmann, I. Sigalas, M. Thiele, M. M. Muller, H. J. Kleebe, A. Michaelis, *Int. J. Refract. Met. H.* **2013**, 39, 53.
[6] E. Amberger, P. Rauh, *Acta Crystallographica Section B: Structural Crystallography and Crystal Chemistry.* **1974**, 30, 2549.
[7] T. Lundstro, Y. G. Andreev, *Materials Science and Engineering: A*. **1996**, 209, 16.
[8] G. Will, K. Kossobutzki, *Journal of the Less Common Metals.* **1976**, 44, 87.
[9] V. L. Solozhenko, Y. Le Godec, O. O. Kurakevych, *Comptes Rendus Chimie.* **2006**, 9, 1472.
[10] K. Shirai, K. Sakuma, N. Uemura, *Phys. Rev. B.* **2014**, 90, 064109 (10 pp.).
[11] G. A. Slack, K. E. Morgan, *Journal of Physics and Chemistry of Solids.* **2014**, 75, 1054.
[12] V. Domnich, S. Reynaud, R. Haber, M. Chhowalla, *J. Am. Ceram. Soc.* **2011**, 94, 3605.
[13] B. M. Moshtaghioun, D. Gomez-Garcia, A. Dominguez-Rodriguez, R. I. Todd, *Journal of the European Ceramic Society.* **2016**, 36, 1829.
[14] M. DeVries, J. Pittari, G. Subhash, K. Mills, C. Haines, J. Q. Zheng, *J. Am. Ceram. Soc.* **2016**, 99, 3398.
[15] V. Mukhanov, O. Kurakevych, V. Solozhenko, *Journal of Superhard Materials.* **2010**, 32, 167.
[16] D. Emin, **1991**, 231, 65.
[17] C. Kunka, A. Awasthi, G. Subhash, *Scr. Mater.* **2017**, 138, 32.
[18] K. Rasim, R. Ramlau, A. Leithe-Jasper, T. Mori, U. Burkhardt, H. Borrmann, W. Schnelle, C. Carbogno, M. Scheffler, Y. Grin, *Angew. Chem. Int. Ed.* **2018**, 130, 1.
[19] V. Adasch, M. Schroeder, D. Kotzott, T. Ludwig, N. Vojteer, H. Hillebrecht, *J. Am. Chem. Soc.* **2010**, 132, 13723.

[20] N. Vojteer, V. Sagawe, J. Stauffer, M. Schroeder, H. Hillebrecht, *Chemistry-A European Journal.* **2011**, 17, 3128.
[21] N. Vojteer, H. Hillebrecht, *Angewandte Chemie International Edition.* **2006**, 45, 165.
[22] G. Subhash, A. Awasthi, C. Kunka, P. Jannotti, M. DeVries, *Scr. Mater.* **2016**, 123, 158.
[23] A. Awasthi, G. Subhash, *Prog. Mater Sci.* **2017**, (accepted).
[24] K. Reddy, A. Hirata, P. Liu, T. Fujita, T. Goto, M. Chen, *Scr. Mater.* **2014**, 76, 9.
[25] M. Chen, J. McCauley, K. Hemker, *Science.* **2003**, 299, 1563.
[26] M. Kolel-Veetil, R. Gamache, N. Bernstein, R. Goswami, S. Qadri, K. Fears, J. Miller, E. Glaser, T. Keller, *J. Phys. Chem. C.* **2015**, 3, 11705.
[27] Q. An, W. Goddard, *J. Phys. Chem. Lett.* **2014**, 5, 4169.
[28] Q. An, W. A. Goddard, *J. Phys. Chem. C.* **2017**, 121, 11831.
[29] N. Vojteer, M. Schroeder, C. Roehr, H. Hillebrecht, *Chemistry-A European Journal.* **2008**, 14, 7331.
[30] T. Ludwig, H. Hillebrecht, *Journal of Solid State Chemistry.* **2006**, 179, 1623.
[31] N. Canter, *Tribol. Lubr. Technol.* **2009**, 65, 14.
[32] V. Ivashchenko, P. E. Turchi, S. Veprek, V. Shevchenko, J. Leszczynski, L. Gorb, F. Hill, *J. Appl. Phys.* **2016**, 119, 205105.
[33] H. Hubert, L. A. Garvie, P. R. Buseck, W. T. Petuskey, P. F. McMillan, *Journal of Solid State Chemistry.* **1997**, 133, 356.
[34] O. O. Kurakevych, V. L. Solozhenko, *Acta Crystallographica Section C: Crystal Structure Communications.* **2007**, 63, i80.
[35] V. L. Solozhenko, O. O. Kurakevych, *Journal of Solid State Chemistry.* **2009**, 182, 1359.
[36] V. Solozhenko, O. Kurakevych, V. Turkevich, D. Turkevich, *Journal of Superhard Materials.* **2009**, 31, 1.
[37] V. L. Solozhenko, V. Z. Turkevich, *arXiv preprint arXiv:1801.00425.* **2018**.
[38] A. Ektarawong, S. Simak, B. Alling, *Physical Review B.* **2017**, 95, 064206.
[39] H. Zhang, S. Yao, M. Widom, *Physical Review B.* **2016**, 93, 144107.
[40] O. O. Kurakevych, V. L. Solozhenko, *Solid State Commun.* **2009**, 149, 2169.
[41] V. Solozhenko, O. Kurakevych, **2008**, 121, 062001.
[42] V. L. Solozhenko, V. Bushlya, *Journal of Superhard Materials.* **2017**, 39, 422.
[43] G. A. Slack, T. McNelly, E. Taft, *Journal of Physics and Chemistry of Solids.* **1983**, 44, 1009.
[44] B. Morosin, A. Mullendore, D. Emin, G. Slack, **1986**, 140, 70.
[45] Z. Liu, J. Kawamura, M. Nagasono, K. Maeda, J. Kawai, *Journal of electron spectroscopy and related phenomena.* **2004**, 135, 73.
[46] C. D. Frye, *B 12 P 2: Improved epitaxial growth and evaluation of a irradiation on its electrical transport properties*, Kansas State University **2016**.
[47] Q. An, W. A. Goddard, *Chem. Mater.* **2015**, 27, 2855.
[48] Q. An, W. A. Goddard III, *The Journal of Physical Chemistry C.* **2017**, 121, 16644.
[49] V. A. Mukhanov, P. S. Sokolov, Y. Le Godec, V. L. Solozhenko, *Journal of Superhard Materials.* **2013**, 35, 415.
[50] V. A. Mukhanov, P. S. Sokolov, O. Brinza, D. Vrel, V. L. Solozhenko, *Journal of Superhard Materials.* **2014**, 36, 18.
[51] Y. Le Godec, M. Mezouar, O. O. Kurakevych, P. Munsch, U. Nwagwu, J. H. Edgar, V. L. Solozhenko, *Journal of Superhard Materials.* **2014**, 36, 61.

[52] V. L. Solozhenko, K. A. Cherednichenko, O. O. Kurakevych, *Journal of Superhard Materials.* **2017**, 39, 71.
[53] H. Bolmgren, T. Lundstrom, S. Okada, *AIP Conference Proceedings.* **1991**, 197.
[54] H. Hubert, L. A. Garvie, B. Devouard, P. R. Buseck, W. T. Petuskey, P. F. McMillan, *Chemistry of materials.* **1998**, 10, 1530.
[55] C. Kunka, Q. An, N. Rudawski, G. Subhash, J. Zheng, V. Halls, J. Singh, *Acta Mater.* **2018**, revision submitted.
[56] D. He, Y. Zhao, L. Daemen, J. Qian, T. D. Shen, T. W. Zerda, **2002**, 81, 643.
[57] Q. An, K. M. Reddy, H. Dong, M. Chen, A. R. Oganov, W. A. Goddard, *Nano Lett.* **2016**, 16, 4236.
[58] H. Dong, A. R. Oganov, Q. Wang, S. N. Wang, Z. Wang, J. Zhang, M. M. Esfahani, X. F. Zhou, F. Wu, Q. Zhu, *Sci. Rep.* **2016**, 6, 31288.
[59] L. Lu, Y. Shen, X. Chen, L. Qian, K. Lu, *Science.* **2004**, 304, 422.
[60] L. Lu, X. Chen, X. Huang, K. Lu, *Science.* **2009**, 323, 607.
[61] N. M. Heckman, M. F. Berwind, C. Eberl, A. M. Hodge, *Acta Mater.* **2018**, 144, 138.
[62] Y. Tian, B. Xu, D. Yu, Y. Ma, Y. Wang, Y. Jiang, W. Hu, C. Tang, Y. Gao, K. Luo, *Nature.* **2013**, 493, 385.
[63] Q. Huang, D. Yu, B. Xu, W. Hu, Y. Ma, Y. Wang, Z. Zhao, B. Wen, J. He, Z. Liu, *Nature.* **2014**, 510, 250.
[64] E. Amberger, P. Rauh, *Acta Crystallographica Section B: Structural Crystallography and Crystal Chemistry.* **1976**, 32, 972.
[65] B. Morosin, T. Aselage, R. Feigelson, *MRS Online Proceedings Library Archive.* **1987**, 97.
[66] A. Ektarawong, S. Simak, B. Alling, *Physical Review B.* **2017**, 96, 024202.
[67] V. Matkovich, *J. Am. Chem. Soc.* **1961**, 83, 1804.
[68] O. Sologub, Y. Matsushita, T. Mori, *Scr. Mater.* **2013**, 68, 289.
[69] H. Bolmgren, T. Lundström, *J. Alloys Compounds.* **1993**, 202, 73.
[70] X. Gonze, *Z. Kristallogr. Cryst. Mater.* **2005**, 220, 558.
[71] X. Gonze, B. Amadon, P. Anglade, J. Beuken, F. Bottin, P. Boulanger, F. Bruneval, D. Caliste, R. Caracas, M. Cote, T. Deutsch, L. Genovese, P. Ghosez, M. Giantomassi, S. Goedecker, D. Hamann, P. Hermet, F. Jollet, G. Jomard, S. Leroux, M. Mancini, S. Mazevet, M. Oliveira, G. Onida, Y. Pouillon, T. Rangel, G. Rignanese, D. Sangalli, R. Shaltaf, M. Torrent, M. Verstraete, G. Zerah, J. Zwanziger, *Comput. Phys. Commun.* **2009**, 180, 2582.
[72] X. Gonze, *Physical Review B.* **1997**, 55, 10337.
[73] X. Gonze, M. Verstraete, C. Audouze, M. Torrent, F. Jollet, *AIP Conference Proceedings.* **2012**, 1504, 944.
[74] X. Gonze, C. Lee, *Physical Review B.* **1997**, 55, 10355.
[75] S. Goedecker, M. Teter, J. Hutter, *Phys. Rev. B.* **1996**, 54, 1703.
[76] C. Kunka, A. Awasthi, G. Subhash, *Scr. Mater.* **2016**, 122, 82.
[77] F. Mouhat, F. Coudert, *Phys. Rev. B.* **2014**, 90, 224104.
[78] J. Wang, J. Li, S. Yip, S. Phillpot, D. Wolf, *Physical Review B.* **1995**, 52, 12627.
[79] J. Wang, S. Yip, S. Phillpot, D. Wolf, *Phys. Rev. Lett.* **1993**, 71, 4182.
[80] Y. P. Lu, D. W. He, **2009**, 105, 083540 (7 pp.).
[81] X. Chen, H. Niu, D. Li, Y. Li, *Intermetallics.* **2011**, 19, 1275.
[82] G. Li, U. Aydemir, S. I. Morozov, S. A. Miller, Q. An, W. A. Goddard III, P. Zhai, Q. Zhang, G. J. Snyder, *Acta Materialia.* **2018**, 149, 341.
[83] G. Kresse, J. Hafner, *Phys. Rev. B.* **1993**, 47, 558.

[84] G. Kresse, J. Furthmüller, *Comput. Mater. Sci.* **1996**, 6, 15.
[85] G. Kresse, J. Furthmüller, *Phys. Rev. B.* **1996**, 54, 11169.
[86] G. Kresse, D. Joubert, *Phys. Rev. B.* **1999**, 59, 1758.
[87] L. Zhong-Li, *Comput. Phys. Commun.* **2015**, 191, 150.
[88] R. B. Kaner, J. J. Gilman, S. H. Tolbert, *Science.* **2005**, 308, 1268.
[89] X. Li, S. Yin, S. H. Oh, H. Gao, *Scr. Mater.* **2017**, 133, 105.

Table I. Relative nanotwinning energies (ΔE_τ), lattice parameters (a), bulk moduli (K), shear moduli (G), microhardness values (HV), shear strengths (τ_{max}), and toughness values (U) are calculated from DFT simulations. Structures are ordered according to the radii of the interstitial atoms (r_i).

Structure	**ΔE_τ**	**r_i**	**a**	**K**	**G**	**HV**	**τ_{max}**	**U**
--	meV	Å	Å	GPa	GPa	GPa	GPa	GJ/m^3
(B_{12})	--	--	5.00	203	145	39	31	8.0
τ-(B_{12})	459	--	5.00	200	143	36	26	3.2
(B_{12})OO	--	0.66	5.10	241	212	37	38	10.4
τ-(B_{12})OO	-3	0.66	5.09	239	214	38	39	10.3
(B_{12})SS	--	1.05	5.29	225	209	22	28	7.2
τ-(B_{12})SS	119	1.05	5.28	221	199	22	30	4.7
(B_{12})PP	--	1.07	5.20	211	196	37	36	8.1
τ-(B_{12})PP	138	1.07	5.21	211	194	37	37	6.2
(B_{12})AsAs	--	1.19	5.25	199	180	34	24	8.3
τ-(B_{12})AsAs	199	1.19	5.27	199	178	33	24	5.8

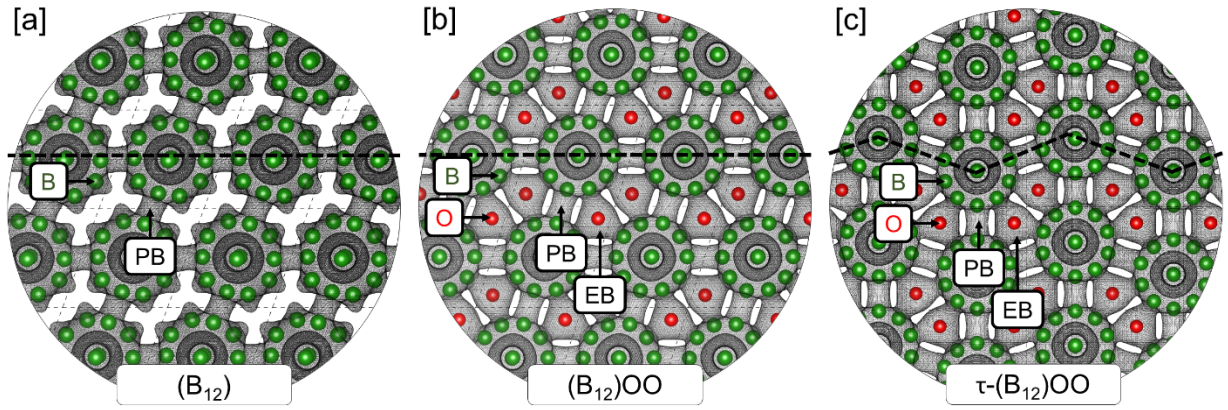

Figure 1. Quantum-mechanical bonding of (a) α-boron [(B_{12})], (b) boron suboxide [$(B_{12})OO$], and (c) nanotwinned boron suboxide [τ-$(B_{12})OO$] are shown along (100). The fundamental structural units of these structures are boron icosahedra directly bonded by polar bonds (PB's). In (b) and (c), icosahedra are also bonded by equatorial bonds (EB's) connecting the icosahedra and interstitial oxygen atoms. In (c), nanotwin boundaries are indicated by bends in the dotted line.

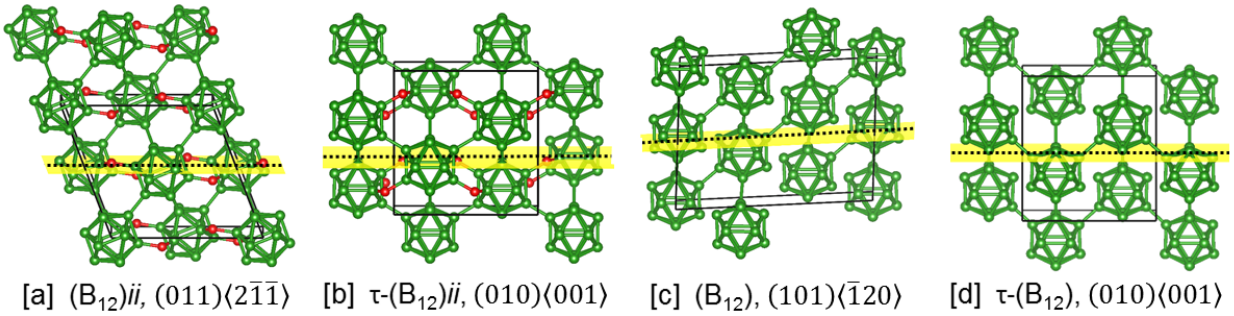

Figure 2. The critical slip systems for pure shear of the nontwinned and nanotwinned (τ) variations of α-boron and boron suboxide (an example hexaboride) are indicated by the dotted lines and yellow planes. Boron and oxygen atoms are represented by green and red spheres, respectively.

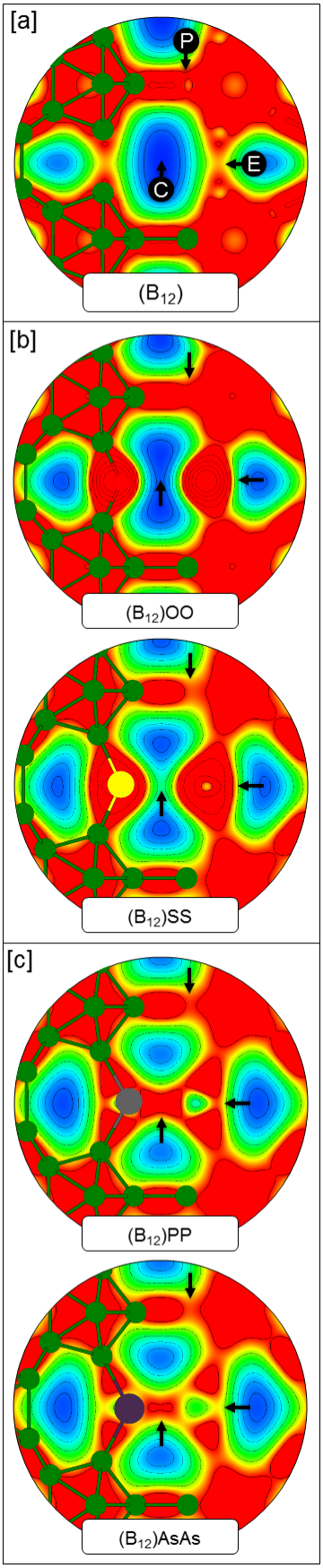
[a]
P
E
C
(B_{12})
[b]
(B_{12})OO
(B_{12})SS
[c]
(B_{12})PP
(B_{12})AsAs

Figure 3. Spatial distributions of electronic density along $(11\bar{1})$ of (a) α-boron, (b) chalcogen hexaborides, and (c) pnictogen hexaborides are indicated by gradients of red (≥0.7 electrons/Å^3) to blue (0 electrons/Å^3). Example polar (P), equatorial (E), and central (C) regions are indicated in (a) and by black arrows. Ball-and-stick models are superimposed on parts of these electronic distributions for clarity and have atomic sizes corresponding to covalent radii.

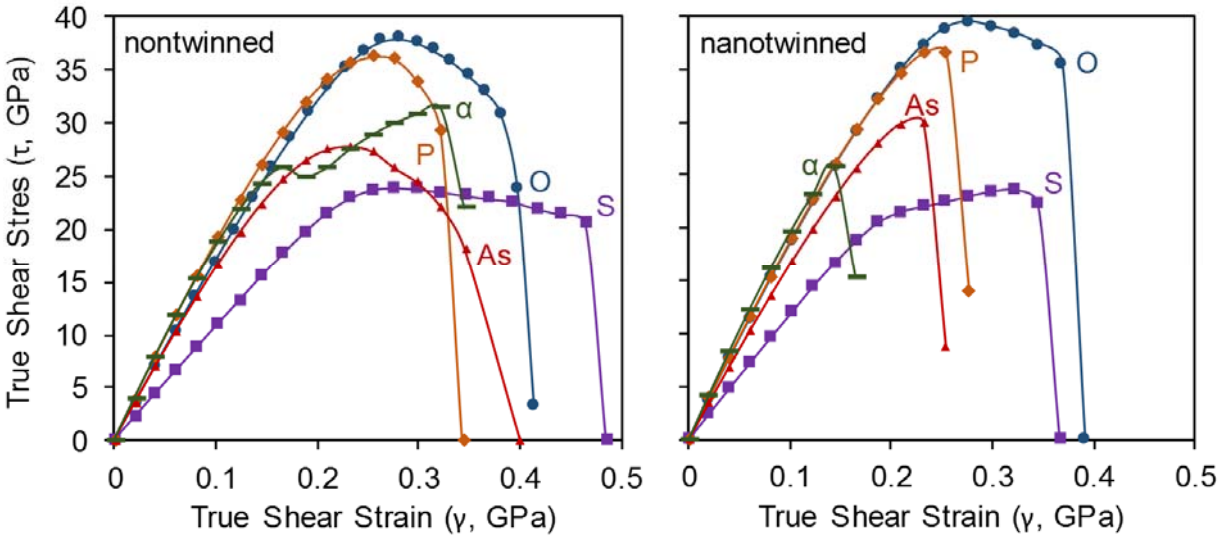

Figure 4. Plots of true stress (τ) versus true strain (γ) are shown for highly-periodic simulations of pure shear of nontwinned and nanotwinned variations of p-block hexaborides and α-boron. With the exception of α-boron (i.e., "α"), curves are labeled according to the interstitial element [e.g., "O" in the nontwinned plot is $(B_{12})OO$].